IMMUNOLOGY

Microglia promote autoimmune inflammation via the noncanonical NF-κB pathway

Zuliang Jie[1,2†], Chun-Jung Ko[1†], Hui Wang[1,3], Xiaoping Xie[1], Yanchuan Li[1], Meidi Gu[1], Lele Zhu[1], Jin-Young Yang[1,4], Tianxiao Gao[1], Wenjuan Ru[5], Shao-Jun Tang[5], Xuhong Cheng[1], Shao-Cong Sun[1,6*]

Microglia have been implicated in neuroinflammatory diseases, including multiple sclerosis and its animal model experimental autoimmune encephalomyelitis (EAE). We demonstrate that microglia mediate EAE disease progression via a mechanism relying on the noncanonical nuclear factor kB (NF-κB) pathway. Microglia-specific deletion of the noncanonical NF-κB-inducing kinase (NIK) impairs EAE disease progression. Although microglial NIK is dispensable for the initial phase of T cell infiltration into the central nervous system (CNS) and EAE disease onset, it is critical for the subsequent CNS recruitment of inflammatory T cells and monocytes. Our data suggest that following their initial CNS infiltration, T cells activate the microglial noncanonical NF-κB pathway, which synergizes with the T cell-derived cytokine granulocyte-macrophage colony-stimulating factor to induce expression of chemokines involved in the second-wave of T cell recruitment and disease progression. These findings highlight a mechanism of microglial function that is dependent on NIK signaling and required for EAE disease progression.

INTRODUCTION

Multiple sclerosis (MS) is a chronic inflammatory disease of the central nervous system (CNS), characterized by accumulation of demyelinating lesions and axonal damage (*1*). A commonly used animal model for studying human MS is experimental autoimmune encephalomyelitis (EAE) (*2*). The pathogenesis of MS and EAE involves activation of myelin-specific $CD4^+$ T cells in peripheral lymphoid organs and their differentiation into inflammatory T helper (T_H) cells, including T_H1 and T_H17 cells (*3*). These autoimmune effector T cells migrate to the CNS, where they are restimulated by local antigen-presenting cells (APCs) displaying myelin-derived antigens and initiate CNS inflammation. The restimulated T cells interact with and activate CNS-resident cells, which causes increased production of proinflammatory cytokines and chemokines, leading to a second wave of T cell and monocytic cell recruitment and disseminated CNS inflammation (*4*, *5*).

Microglia are CNS-resident macrophages implicated in the pathogenesis of MS and EAE (*6*–*8*). Unlike the peripheral monocytes and macrophages, which are short-lived and continuously replaced by bone marrow precursor cells, microglia are derived from yolk sac and maintained through self-renewal in the CNS (*9*–*11*). During EAE induction, microglia secrete chemokines and proinflammatory cytokines that mediate leukocyte recruitment into the CNS and promote inflammation (*7*, *12*). However, the molecular mechanism by which microglia cross-talk with T cells and participate in EAE induction is incompletely understood. The signaling network mediating microglial activation and pathological function is also poorly defined.

The nuclear factor κB (NF-κB) family of transcription factors has been associated with various inflammatory diseases (*13*). NF-κB activation is mediated by canonical and noncanonical pathways, which differ in both signaling mechanisms and biological functions (*14*). The noncanonical NF-κB pathway is based on signal-induced processing of the NF-κB2 precursor protein p100, a process leading to generation of the mature NF-κB2 p52 and nuclear translocation of p100-sequestered NF-κB members, p52 and RelB (*15*). A central component of the noncanonical NF-κB pathway is NF-κB–inducing kinase (NIK), which, along with its downstream kinase, inhibitor of NF-κB kinase α, mediates phosphorylation-dependent p100 processing (*16*, *17*). Under steady-state conditions, NIK is subject to ubiquitin-dependent degradation mediated by an E3 ubiquitin ligase complex, composed of cellular inhibitor of apoptosis (cIAP), tumor necrosis factor receptor (TNFR)–associated factor 2 (TRAF2), and TRAF3; signal-induced noncanonical NF-κB activation typically involves TRAF3 degradation and NIK accumulation (*15*). Well-defined immune receptors targeting the noncanonical NF-κB pathway include a subset of TNFR superfamily members, such as CD40, B cell-activating factor receptor (BAFFR), lymphotoxin-β receptor (LTβR), and receptor activator of NF-κB (RANK) (*14*). The noncanonical NF-κB pathway regulates important immune processes, including lymphoid organ development and B cell maturation (*14*, *18*). However, the role of this signaling pathway in regulating the function of tissue-resident cells, particularly microglia, in inflammatory disorders is not well understood.

In the present study, we demonstrate that the noncanonical NF-κB pathway is activated in microglia during EAE induction, where it mediates induction of chemokines and recruitment of inflammatory T cells to the CNS for EAE disease progression. Our data suggest that the noncanonical NF-κB pathway in microglia responds to inflammatory T cells and mediates chemokine gene induction in synergy with a T cell–derived cytokine, granulocyte-macrophage colony-stimulating factor (GM-CSF). These findings demonstrate a

[1]Department of Immunology, University of Texas MD Anderson Cancer Center, Houston TX, USA. [2]State Key Laboratory of Cellular Stress Biology, Innovation Center for Cell Biology, School of Life Sciences, Xiamen University, Xiamen, China. [3]Jiangsu Key Laboratory of Immunity and Metabolism, Department of Pathogenic Biology and Immunology, Xuzhou Medical University, Xuzhou, China. [4]Department of Biological Sciences, Pusan National University, Busan, South Korea. [5]Department of Neuroscience and Cell Biology, University of Texas Medical Branch, Galveston, TX, USA. [6]MD Anderson Cancer Center UT Health Graduate School of Biomedical Sciences, Houston, TX, USA.
*Corresponding author. Email: ssun@mdanderson.org
†These authors contributed equally to this work as co-first authors.

novel mechanism underlying microglial activation and function in CNS inflammation and identify NIK as an important mediator of the T cell–microglial cell interplay.

RESULTS

EAE induction is associated with noncanonical NF-κB activation in microglia

To assess the involvement of noncanonical NF-κB pathway in microglial function, we analyzed p100 processing during EAE induction by immunization of mice with a myelin oligodendrocyte glycoprotein (MOG) peptide ($MOG_{35–55}$) along with pertussis toxin. The microglia of the untreated mice had a low basal level of p100 processing, as detected on the basis of generation of the mature NF-κB2 p52 (Fig. 1A). A much higher level of p52 was detected in both the whole-cell lysates and nuclear extracts of microglia isolated from day 20 EAE mice (Fig. 1A). A time course study revealed that induction of p100 processing was weak on day 10 but profoundly increased on day 20 after EAE induction (Fig. 1B). These results suggest that the noncanonical NF-κB pathway is activated with delayed kinetics along with EAE induction.

NIK deficiency in microglia ameliorates late-phase EAE

To investigate microglia-specific function of the noncanonical NF-κB in EAE pathogenesis, we generated mice with microglia-conditional deletion of the NIK-encoding gene, *Map3k14*, using a previously defined approach (*19*). Briefly, we crossed *Map3k14* flox mice with *Cx3Cr1*$^{CreER\text{-}eYFP}$ transgenic mice and injected the *Map3k14*$^{fl/fl}$*Cx3cr1*$^{CreER\text{-}eYFP}$ and *Map3k14*$^{+/+}$*Cx3cr1*$^{CreER\text{-}eYFP}$ mice with tamoxifen (for Cre induction), followed by 25 days of housing without tamoxifen injection, to obtain *Map3k14* microglia-conditional knockout (*Map3k14*-cKO) and wild-type control mice (fig. S1A). This approach is based on the fact that peripheral monocytes are short-lived and replaced by wild-type bone marrow precursors, whereas microglia are long-lived and self-renewed (*19*). Thus, 25 days after tamoxifen injection, Cre [enhanced yellow fluorescent protein (eYFP)] expression was retained in the CNS microglia but not in monocytes of the peripheral lymphoid organs, spleen, and lymph nodes (fig. S1B). Quantitative reverse transcription polymerase chain reaction (qRT-PCR) confirmed *Map3k14* deletion in microglia but not in peripheral monocytes or T cells (fig. S1C).

The conditional NIK deficiency did not alter the frequency of CNS microglia or their surface activation markers under steady

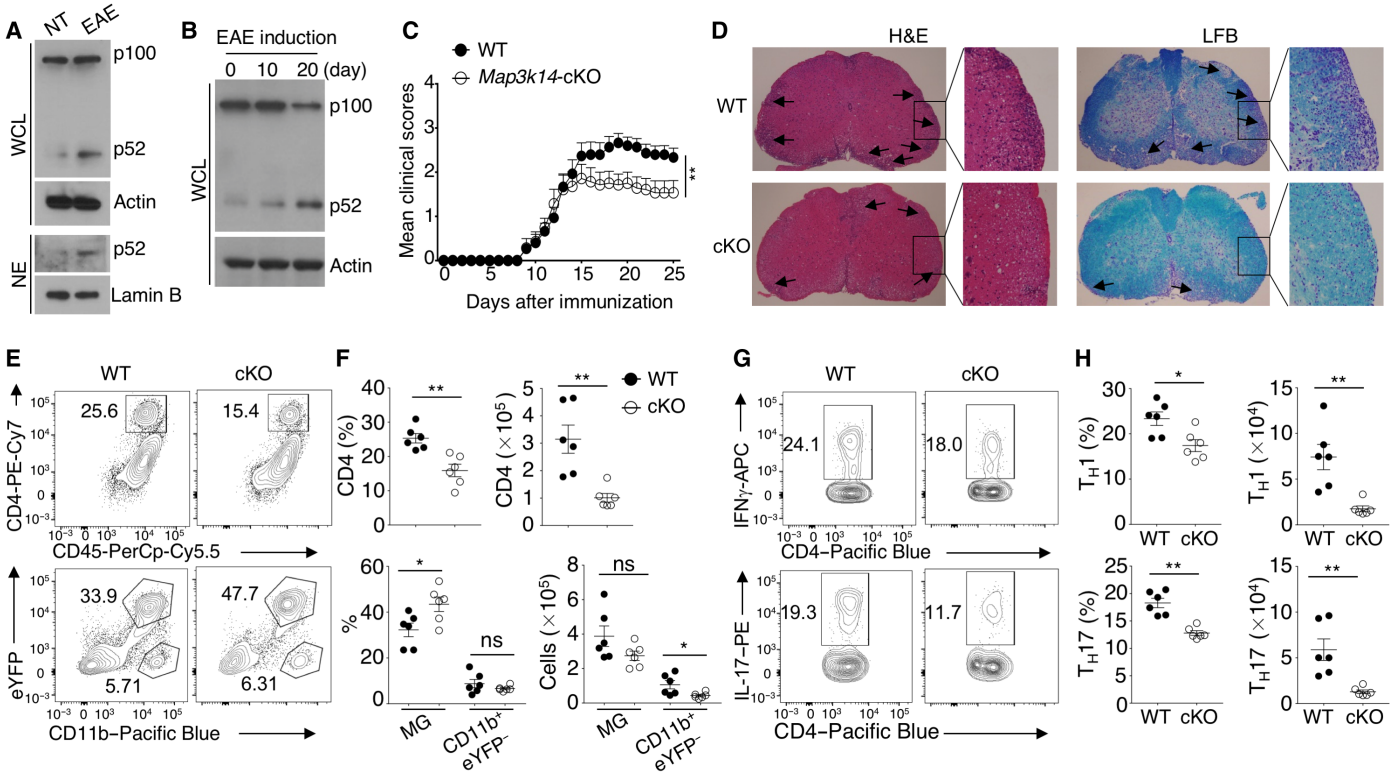

Fig. 1. Microglial NIK is required for EAE disease progression but not initiation. (**A** and **B**) Immunoblot analysis of the indicated proteins in whole-cell lysates (WCL) and nuclear extracts (NE) of microglia freshly isolated from nontreated (NT) and EAE-induced (day 20 after immunization) mice (A) or from mice at the indicated time points of EAE induction (B). (**C**) Mean clinical scores of age- and sex-matched wild-type (WT) and *Map3k14*-cKO mice subjected to $MOG_{35–55}$-induced EAE ($n = 14$ per group). (**D**) Hemotoxylin and eosin (H&E) and Luxol Fast Blue (LFB) staining of spinal cord sections from $MOG_{35–55}$-immunized (day 25) WT and *Map3k14*-cKO mice for visualizing immune cell infiltration and demyelination, respectively (arrows). (**E** and **F**) Flow cytometric analysis of $CD4^+$ T cells, $eYFP^-CD11b^+$ monocytes, and $eYFP^+CD11b^+$ microglia (MG) in the CNS (brain and spinal cord) of $MOG_{35–55}$-immunized WT and *Map3k14*-cKO mice ($n = 6$, day 25 after immunization). Data are presented as a representative plot (E) and summary graph (F). (**G** and **H**) Flow cytometry and intracellular cytokine staining (ICS) analysis of interferon-γ (IFNγ)–producing T_H1 cells and interleukin-17 (IL-17)–producing T_H17 cells in the CNS of $MOG_{35–55}$-immunized WT and *Map3k14*-cKO mice ($n = 6$, day 25 after immunization). Data are presented as a representative plot (G) and summary graph (H). Data are representative of three independent experiments. Summary data are presented as means ± SEM with *P* values determined by two-way analysis of variance (ANOVA) analysis (C) or unpaired two-tailed Student's *t* test (F and H). $^*P < 0.05$ and $^{**}P < 0.01$. ns, not significant.

conditions (fig. S1, D and E). Furthermore, *Map3k14*-cKO and wild-type mice had comparable disease severity during early-phase EAE (Fig. 1C). However, the late-phase EAE was notably ameliorated in the *Map3k14*-cKO mice, coupled with substantially reduced immune cell infiltration and demyelination in the CNS (Fig. 1, C and D). Parallel flow cytometric analyses revealed that during the late-phase EAE induction, the *Map3k14*-cKO mice had a profoundly lower frequency and absolute number of CNS-infiltrating $CD4^+$ T cells, as well as T_H1 and T_H17 effector T cells, compared to the wild-type control mice (Fig. 1, E to H). The absolute number, although not frequency, of infiltrating monocytes ($CD11b^+eYFP^-$) was also reduced in the *Map3k14*-cKO mice (Fig. 1, E and F). On the other hand, the cKO mice displayed an increased frequency of microglia ($eYFP^+CD11b^+$); however, this result was apparently due to reduced CNS-infiltrating immune cells since the absolute number of microglia was comparable between the wild-type and cKO mice (Fig. 1, E and F).

Since microglia-specific NIK deficiency had no effect on early-phase EAE induction (Fig. 1C), we examined T cell infiltration into the CNS during early-phase EAE. On day 12 of EAE induction, the *Map3k14*-cKO and wild-type mice had comparable frequencies of CNS-infiltrating $CD4^+$ T cells, as well as T_H1 and T_H17 effector T cells (fig. S2, A and B). The frequency of $eYFP^+$ microglia and the $eYFP^-$ CNS-infiltrating monocytes of the cKO and wild-type mice was also similar (fig. S2C). These results were consistent with the comparable disease severity of the cKO and wild-type mice during the early phase of EAE induction (Fig. 1C). Collectively, these results suggest that NIK functions in microglia to regulate the abundance of CNS-infiltrating T cells and EAE pathogenesis during the late phase.

Microglial NIK is required for CNS recruitment of T cells during EAE progression

Induction of EAE involves generation of myelin-specific T_H1 and T_H17 cells in the draining lymph node and their infiltration into the CNS. We found that the *Map3k14*-cKO and wild-type mice had comparable frequencies of T_H1 and T_H17 effector T cells and regulatory T cells in the draining lymph node, suggesting normal activation and differentiation of $CD4^+$ T cells (Fig. 2A). The wild-type and *Map3k14*-cKO lymph node T cells also expressed a comparable level of chemokine receptors, CXCR3, CCR5, and CCR6 (Fig. 2B),

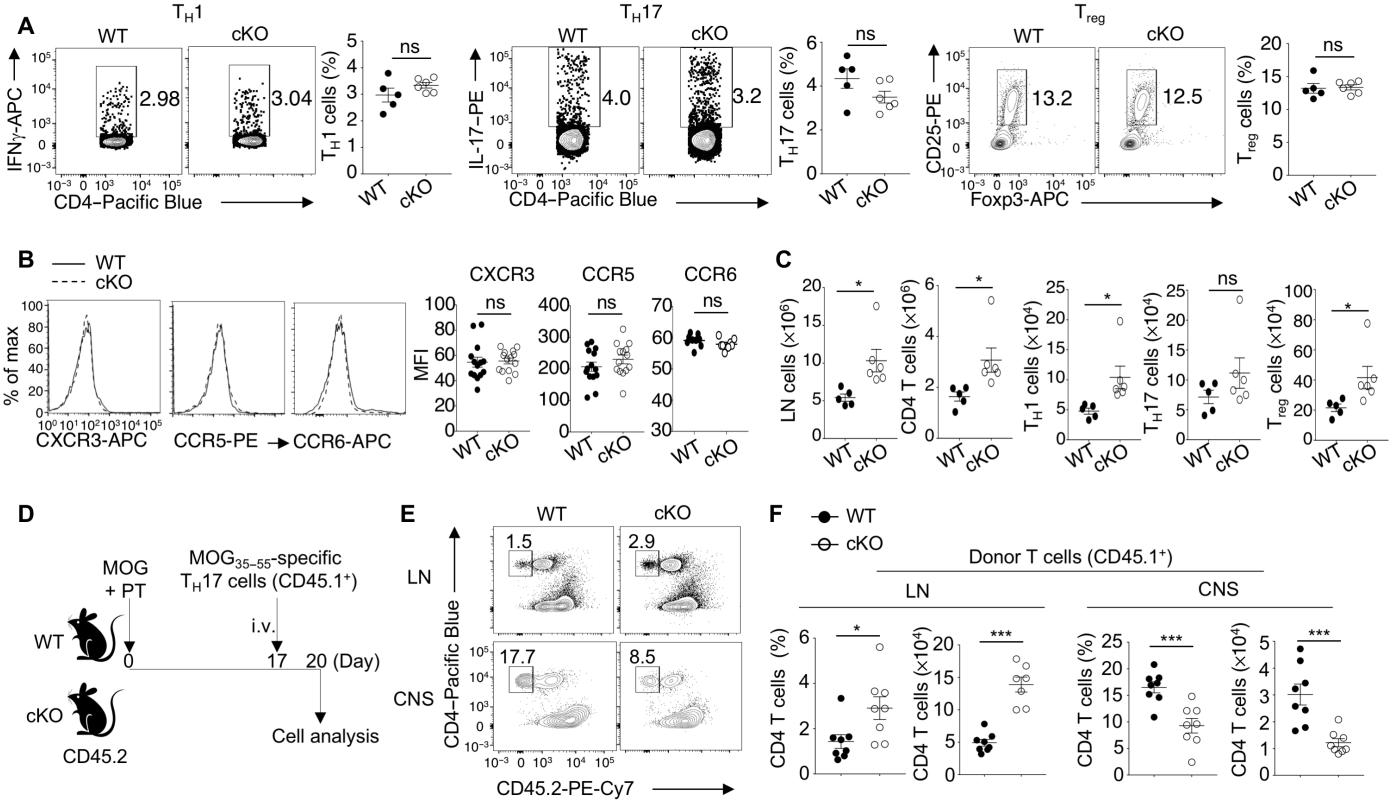

Fig. 2. NIK deletion in microglia has no effect on T cell activation but impairs T cell recruitment to the CNS. (**A**) Flow cytometric analysis of IFNγ-producing T_H1 cells, IL-17–producing T_H17 cells, and $CD25^+Foxp3^+$ regulatory T (T_{reg}) cells in the draining lymph nodes of MOG_{35-55}-immunized wild-type and *Map3k14*-cKO mice (day 25 after immunization). Data are presented as representative plots (left) and summary graphs (right). (**B**) Flow cytometric analysis of chemokine receptors on draining lymph node $CD4^+$ T cells of MOG_{35-55}-immunized wild-type and *Map3k14*-cKO mice. Data are presented as a representative plot (left) and summary graph (right). MFI, mean fluorescence intensity. (**C**) Absolute cell numbers of total lymphocytes, $CD4^+$ T cells, and T_H1, T_H17, and regulatory T cell subsets of $CD4^+$ T cells in the draining lymph nodes (LNs) of MOG_{35-55}-immunized wild-type and *Map3k14*-cKO mice (wild-type, $n = 5$; cKO, $n = 6$; day 25 after immunization). (**D**) Schematic of experimental design. MOG_{35-55}-specific T_H17 cells (1×10^6 cells) from B6.SJL ($CD45.1^+$) mice were adoptively transferred to day 17 of EAE-induced (MOG_{35-55} plus pertussis toxin) wild-type and *Map3k14*-cKO ($CD45.2^+$) mice, and donor $CD4^+$ T cells were analyzed 3 days after transfer. i.v., intravenously. (**E** and **F**) Flow cytometric analysis of donor $CD4^+$ T cells ($CD45.2^-$) in inguinal lymph node and CNS of the T_H17 recipient mice depicted in (F). Data are presented as a representative plot (E) and summary graphs (F). Data are representative of two (D to F) and three (A to C) independent experiments, and *P* values were determined by two-tailed Student's *t* test. $^*P < 0.05$ and $^{***}P < 0.01$.

known to mediate T cell migration into site of inflammation (*20*–*24*). Notably, the absolute number of lymph node $CD4^+$ T cells was increased in the *Map3k14*-cKO mice compared to that of wild-type mice (Fig. 2C). These results, along with the marked reduction in the CNS-infiltrating T cells in the cKO mice (Fig. 1, E to H), indicate that NIK may function in microglia to mediate recruitment of encephalitogenic T cells to the CNS.

To further determine whether microglial NIK mediates the recruitment of T cells into the CNS during EAE disease progression, we adoptively transferred $MOG_{35–55}$-specific T_H17 cells derived from B6.SJL mice ($CD45.1^+$) to EAE-induced wild-type or *Map3k14*-cKO recipient mice (Fig. 2D). After 3 days of adoptive transfer, the donor $CD4^+$ T cells ($CD45.2^–$) were efficiently recruited to the CNS in wild-type recipient mice, but much less efficiently recruited to the CNS of *Map3k14*-cKO recipient mice (Fig. 2, E and F). This result was associated with profound accumulation of donor $CD4^+$ T cells in the draining lymph node of the *Map3k14*-cKO recipient mice (Fig. 2, E and F), emphasizing a crucial role for the microglial NIK in mediating CNS recruitment of inflammatory T cells during EAE disease progression.

NIK ablation in microglia impairs microglial activation and chemokine expression

Our finding that microglial NIK is required for T cell recruitment to the CNS during late-phase EAE prompted us to examine whether the NIK signaling pathway mediates microglia activation and cytokine production. We found that NIK deficiency impaired the processing of p100 in microglia along with EAE induction (Fig. 3A). We next analyzed microglial activation based on surface expression of well-defined activation markers, including major histocompatibility complex II (MHCII), CD80, CD86, and CD45. Although NIK deficiency had no effect on the basal level expression of MHCII, CD80, CD86, and CD45 in untreated mice (fig. S1E), it attenuated the expression of these activation markers during EAE induction (Fig. 3, B and C). Furthermore, this result was due to a cell-intrinsic function of NIK, since the microglia-conditional NIK deficiency did not affect expression of the activation markers on the CNS-infiltrating $eYFP^–CD11b^+$ monocytes (Fig. 3, D and E). Consistent with these results, immunofluorescence assays revealed that the spinal cord of *Map3k14*-cKO EAE mice had reduced expression of ionized calcium-binding adapter molecule 1 (Iba1), a microglial marker

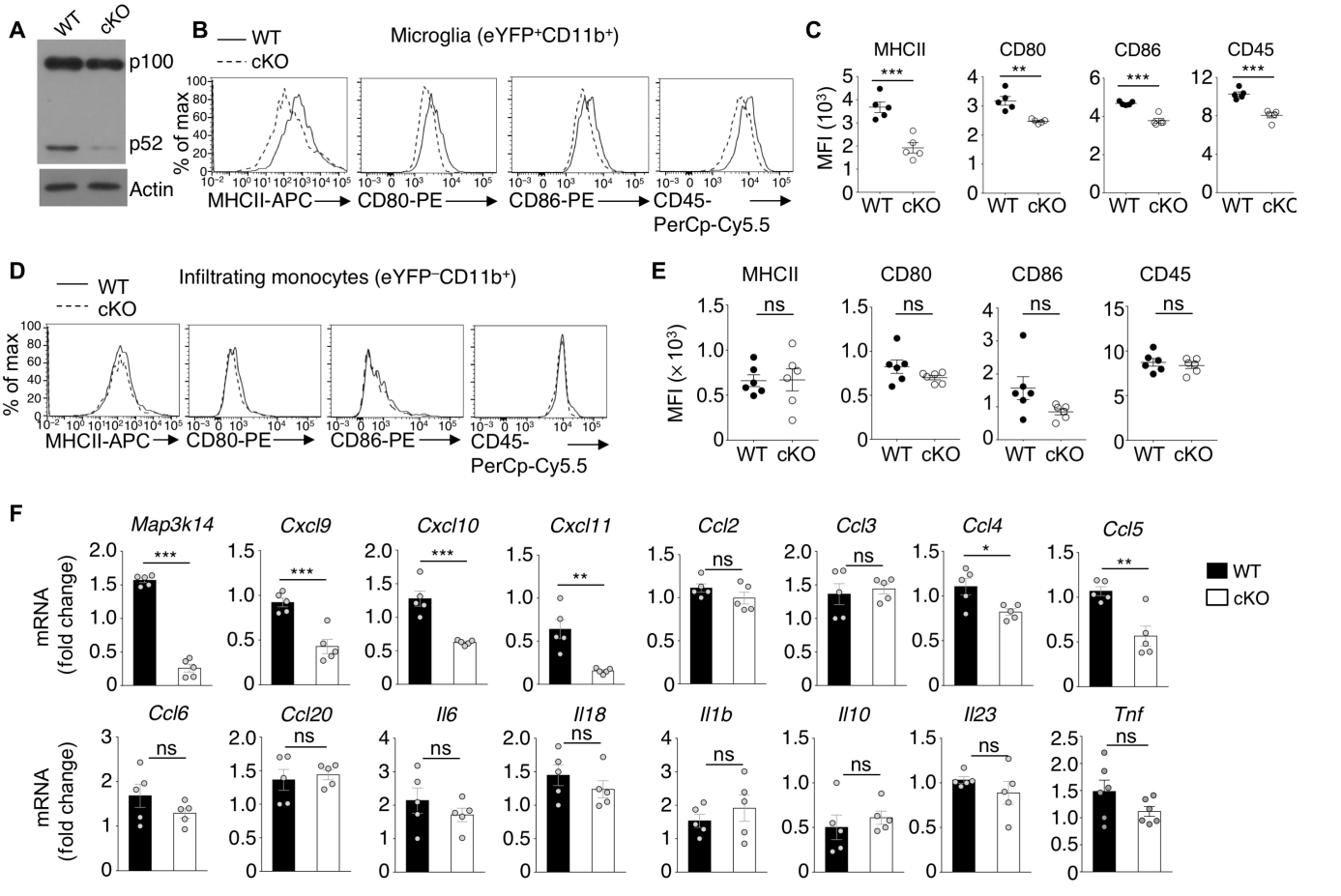

Fig. 3. NIK facilitates microglial activation and chemokine induction in EAE. (**A**) Immunoblot analysis of p100 and p52 in whole-cell lysates of sorted microglia ($CD11b^+eYFP^+$ cells) from the CNS of $MOG_{35–55}$-immunized (day 25) WT and *Map3k14*-cKO mice. (**B** to **E**) Flow cytometric analysis of surface activation markers in the $eYFP^+CD11b^+$ microglia (B and C) and the $eYFP^–CD11b^+$ monocytes (D and E) of EAE-induced WT and *Map3k14*-cKO mice. Data are presented as representative plots (B and D) and summary graphs (C and E). (**F**) qRT-PCR analysis of the indicated mRNAs in freshly sorted microglia from $MOG_{35–55}$-immunized WT and *Map3k14*-cKO mice ($n = 5$ per genotype, day 25 after immunization). Data are representative of two (A) or three (B to F) independent experiments. Summary data are presented as means ± SEM based on multiple mice, with *P* values determined by two-tailed Student's *t* test. $^*P < 0.05$, $^{**}P < 0.01$, and $^{***}P < 0.001$.

protein up-regulated along with EAE-mediated microglial activation (fig. S3, A and B).

The recruitment of T cells into tissues, including the CNS, is critically dependent on chemokines produced at the sites of inflammation (*21*, *22*). qRT-PCR analysis revealed the expression of a number of chemokines and cytokines in microglia freshly isolated from EAE-induced mice (Fig. 3F). The expression of several chemokine genes, including *Cxcl9*, *Cxcl10*, *Cxcl11*, *Ccl4*, and *Ccl5*, were significantly reduced in the NIK-deficient microglia (Fig. 3F). Notably, Cxcl9, Cxcl10, and Cxcl11 are ligands of the chemokine receptor Cxcr3, which mediates recruitment of effector T cells to site of inflammation, including the CNS in MS and EAE (*21*, *22*). Ccl4 and Ccl5 are ligands of CCR5, which is involved in recruitment of inflammatory T cells and monocytic cells to the CNS during EAE (*23*, *24*). CCR6 is also known to mediate T_H17 cell entry into the CNS (*20*), but the expression of its ligand, Ccl20, in microglia was not influenced by NIK deficiency (Fig. 3F). NIK was also dispensable for microglial expression of several proinflammatory cytokines during EAE induction (Fig. 3F). However, analysis of the spinal cord tissue in EAE mice revealed reduced expression of several proinflammatory cytokines, as well as chemokines, in the *Map3k14*-cKO mice compared to wild-type mice (fig. S3C). This latter finding was in line with the reduced CNS infiltration with inflammatory immune cells (Fig. 1, D to F), which also produce inflammatory mediators. Notwithstanding, these results demonstrate a crucial role for the NIK signaling pathway in mediating chemokine induction in microglia, providing mechanistic insight into the microglial cell–specific function of NIK in regulating EAE pathogenesis.

NIK signaling axis mediates T cell–induced microglial activation and passive EAE

Induction of EAE involves an initial phase of CNS infiltration with encephalitogenic T effector cells, where they are thought to activate CNS-resident cells to trigger a second wave of recruitment of T cells and monocytes, causing disseminated CNS inflammation (*4*, *5*). Our data suggested that microglial NIK was required for CNS recruitment of T cells during the late phase, but not the initial phase, of EAE (Fig. 1, E to H, and fig. S2). These results, along with the finding that NIK mediated microglial activation, raised the question of whether NIK might mediate microglial activation by the infiltrating T cells. To test this possibility, we performed passive EAE induction by adoptive transfer of activated $MOG_{35–55}$-specific T_H17 cells from B6.SJL mice ($CD45.1^+$) into sublethally irradiated wild-type or *Map3k14*-cKO mice (Fig. 4A). The *Map3k14*-cKO recipient mice were fully susceptible to passive EAE induction during the early phase (Fig. 4A), further suggesting a dispensable role of microglial NIK in the initial phase of T cell recruitment and EAE induction. In contrast, the late-phase EAE was profoundly ameliorated in the *Map3k14*-cKO recipient mice (Fig. 4A), which was associated with significantly reduced CNS infiltration with the donor $CD4^+$ T cells ($CD45.1^+$) and T_H17 effector T cells (Fig. 4, B and C).

To further define the mechanism by which microglial NIK mediates T_H17 cell–induced EAE, we examined the noncanonical NF-κB signaling in microglia. Adoptive transfer of $MOG_{35–55}$-specific T_H17 cells significantly induced p100 processing to p52 in microglia, which was largely abolished in the *Map3k14*-cKO mice (Fig. 4D). The p100 processing was also induced in microglia cocultured with activated T cells in vitro (Fig. 4E), suggesting that the NIK signaling pathway responds to T cell–mediated microglial activation. NIK ablation in microglia significantly reduced the expression levels of several microglial activation markers in the T_H17 cell–induced passive EAE, including MHCII, CD80, CD86, and CD45 (Fig. 4F). Furthermore, the NIK deficiency attenuated the expression of microglial chemokines, *cxcl9*, *cxcl10*, and *cxcl11*, during the passive EAE induction (Fig. 4G). Collectively, these data suggest that the NIK signaling pathway responds to T cells in microglia and mediates induction of chemokines involved in T cell recruitment into the CNS for EAE disease progression.

Noncanonical NF-κB mediates chemokine induction in synergy with GM-CSF

Typical receptors targeting the noncanonical NF-κB pathway are TNFR superfamily members, including LTβR, RANK, BAFFR, CD40, and TNFR2 (*14*). Flow cytometry detected expression of several TNFRs in microglia of EAE-induced mice, particularly LTβR and RANK (Fig. 5A). Microglia displayed a basal level expression of LTβR and RANK (day 0 of EAE induction), and the expression level of RANK and, to a less extent, LTβR was up-regulated along the course of EAE induction (Fig. 5B). Naïve microglia prepared from untreated newborn mice and cultured in vitro also displayed a basal level expression of LTβR and RANK, as well as TNFR2 and CD40 (fig. S4). Notably, the ligands for LTβR (LTα1β2 and LIGHT), RANK (RANKL), TNFR2 (TNFα), and CD40 (CD40L) are expressed on activated T cells (*25*, *26*). We found that in vitro stimulation of microglia with an agonistic LTβR antibody (anti-LTβR) or RANKL resulted in the induction of p100 processing and nuclear p52 expression, which was abolished in the NIK-deficient microglia (Fig. 5C).

To assess the role of the noncanonical NF-κB pathway in chemokine gene induction, we stimulated the microglia with anti-LTβR and RANKL. Stimulation of microglia with anti-LTβR or RANKL did not significantly induce chemokine gene expression (Fig. 5D), suggesting the requirement of a costimulatory signal. In this regard, encephalitogenic T_H1 and T_H17 cells produce a proinflammatory cytokine, GM-CSF, which is critical for the microglial activation and EAE induction (*27*–*29*). Our flow cytometry analysis also revealed up-regulated GM-CSF expression in CNS-infiltrating CD4 T cells along with EAE induction (fig. S5). We thus examined whether the noncanonical NF-κB inducers might synergize with this inflammatory cytokine in chemokine induction. GM-CSF alone only weakly stimulated the expression of *Cxcl9*, *Cxcl10*, and *Cxcl11* in microglia; however, when combined with either anti-LTβR or RANKL, GM-CSF potently induced the expression of these chemokines (Fig. 5D). Unlike GM-CSF, interleukin-17 (IL-17) did not synergize with anti-LTβR or RANKL in chemokine induction (fig. S6A). Induction of chemokine gene expression by GM-CSF and noncanonical NF-κB inducers was dependent on NIK, since it was attenuated in the *Map3k14*-cKO microglia (Fig. 5E). Furthermore, chromatin immunoprecipitation (ChIP) assays revealed the binding of noncanonical NF-κB members, RelB and p52, to the promoter region of the *Cxcl10* gene (Fig. 5F), suggesting the direct involvement of noncanonical NF-κB in mediating chemokine gene induction. Parallel experiments revealed that NIK deficiency did not influence the induction of microglial gene expression by the Toll-like receptor 4 agonist lipopolysaccharide (fig. S6B).

To further examine the role of noncanonical NF-κB in NIK-mediated chemokine induction, we used a mouse model, $Nfkb2^{lym1}$, expressing a p100 mutant lacking its C-terminal phosphorylation residues and, thus, defective in signal-induced processing (*30*).

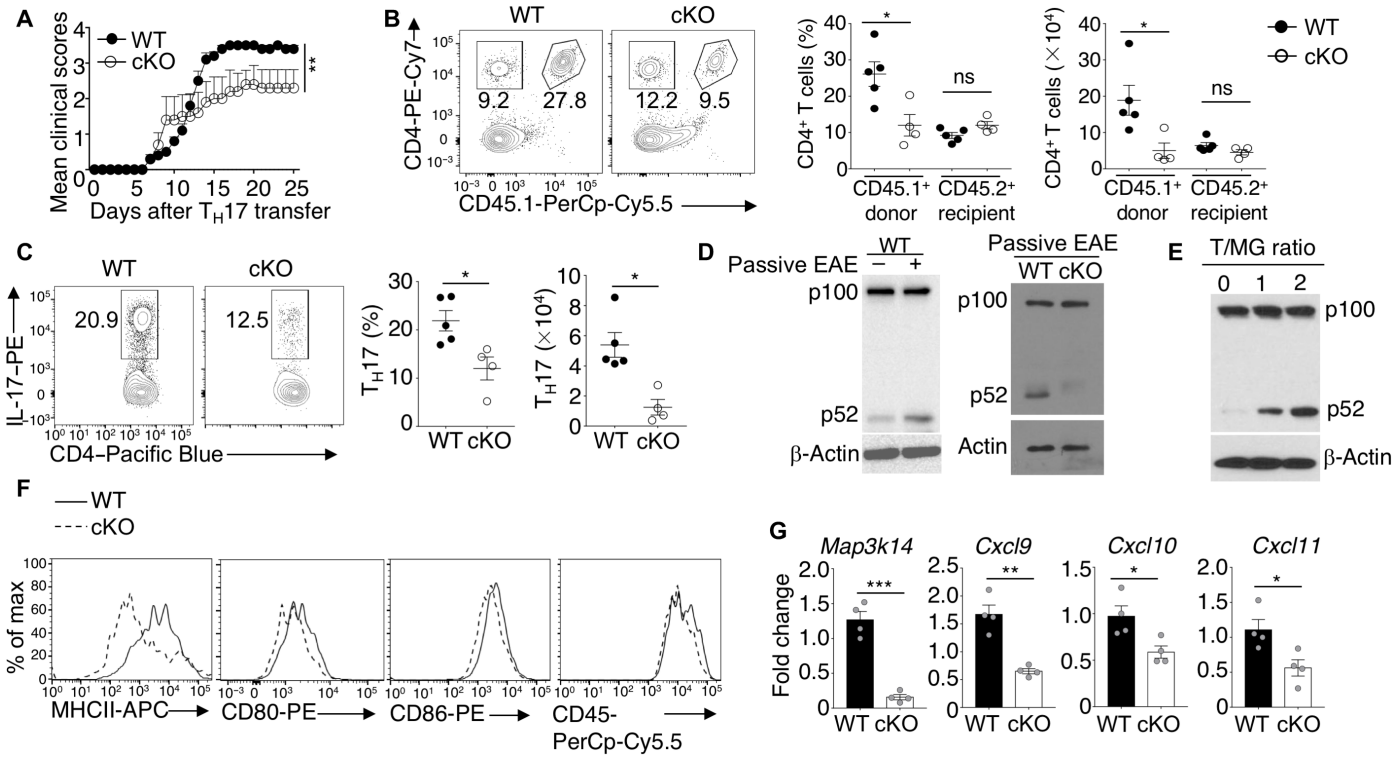

Fig. 4. NIK mediates T cell–induced microglial cell activation passive EAE. (**A**) Passive EAE clinical scores of WT and *Map3k14*-cKO (cKO) recipient mice adoptively transferred with $CD45.1^+$ $MOG_{35–55}$-specific T_H17 cells (2×10^6 cells). (**B** and **C**) Flow cytometric analysis of donor ($CD45.1^+$) and recipient ($CD45.1^-$) $CD4^+$ T cells (B) and T_H17 cells (C) in the CNS (brain and spinal cord) of passive EAE–induced (day 25 after T_H17 cell–adoptive transfer) WT and *Map3k14*-cKO mice. Data are presented as a representative plot (left) and summary graph (right). (**D**) Immunoblot analysis of the indicated proteins in whole-cell extracts of microglia ($CD11b^+eYFP^+$ cells) freshly isolated from wild-type or *Map3k14*-cKO mice that were either not treated (–) or treated (+) with T_H17 cell–induced passive EAE. (**E**) Immunoblot analysis of the indicated proteins in whole-cell extracts of microglia cocultured for 24 hours with activated T cells in the indicated T cell–to–microglia (T/MG) ratios. (**F**) Flow cytometric analysis of surface activation markers in microglia of passive EAE–induced WT and *Map3k14*-cKO mice. (**G**) qRT-PCR analysis of the indicated mRNAs in freshly sorted microglia ($CD11b^+eYFP^+$ cells) from the CNS of passive EAE–induced wild-type and *Map3k14*-cKO mice. Data are representative of two independent experiments. Summary data are presented as means ± SEM, and *P* values were determined by two-way ANOVA analysis (A) or two-tailed Student's *t* test (B, C, and G). $^*P < 0.05$, $^{**}P < 0.01$, and $^{***}P < 0.001$.

Because of dominant expression of the mutant *Nfkb2* allele, even the *Nfkb2*$^{lym1/+}$ heterozygous mice display severe defect in p100 processing in B cells (*30*). Induction of p100 processing and p52 nuclear translocation by anti-LTβR and RANK was impaired in the *Nfkb2*$^{lym1/+}$ microglia (Fig. 5, G and H). Similar to the NIK-deficient microglia, the *Nfkb2*$^{lym1/+}$ microglia displayed a defect in chemokine induction (Fig. 5I), thus confirming a role for the noncanonical NF-κB pathway in mediating microglial chemokine gene induction.

We next performed passive EAE by adoptive transfer of $MOG_{35–55}$-specific T_H17 cells into sublethally irradiated *Nfkb2*$^{lym1/+}$ or wild-type control mice (fig. S7A). The *Nfkb2*$^{lym1/+}$ mice displayed markedly reduced severity of passive EAE as compared to their wild-type counterparts (fig. S7B). Furthermore, passive EAE–induced p100 processing was impaired in the microglia of *Nfkb2*$^{lym1/+}$ recipient mice (fig. S7C). The impaired noncanonical NF-κB activation was associated with attenuated chemokine gene expression and activation marker expression in the microglia of *Nfkb2*$^{lym1/+}$ passive EAE mice (fig. S7, D and E). These results suggest that inflammatory T cells may stimulate NIK-dependent activation of noncanonical NF-κB, which in turn mediates microglial cell activation and chemokine expression.

TRAF3 deficiency in microglia exacerbates CNS inflammation in an NIK-dependent manner

TRAF3 has been implicated as a negative regulator of EAE induction (*12*, *31*); however, whether and how TRAF3 functions in microglia to regulate EAE pathogenesis remain unclear. To determine the microglial cell–specific function of TRAF3, we generated microglial cell–conditional *Traf3* KO (*Traf3*-cKO) and wild-type control mice by injecting the *Traf3*$^{fl/fl}$*Cx3Cr1*^{CreErt2} and *Traf3*$^{+/+}$*Cx3Cr1*^{CreErt2} mice with tamoxifen and subsequently housing for 25 days without tamoxifen injection. As expected, Traf3 was deleted in the $eYFP^+$ microglia but not in the $eYFP^-$ cells (Fig. 6A). The microglial cell–specific Traf3 deficiency did not influence the disease onset but significantly exacerbated the disease progression in MOG-induced EAE (Fig. 6B). The exacerbated EAE disease severity in the *Traf3*-cKO mice was associated with an increased frequency and absolute number of CNS-infiltrating $CD4^+$ T cells, as well as T_H1 and T_H17 effector T cells (Fig. 6, C and D). The Traf3 deficiency did not significantly alter the number of microglia, although the relative frequency of microglia was reduced in the *Traf3*-cKO mice apparently due to the increased CNS-infiltrating T cells (Fig. 6E). These results suggest a microglial cell–intrinsic function of Traf3 in the

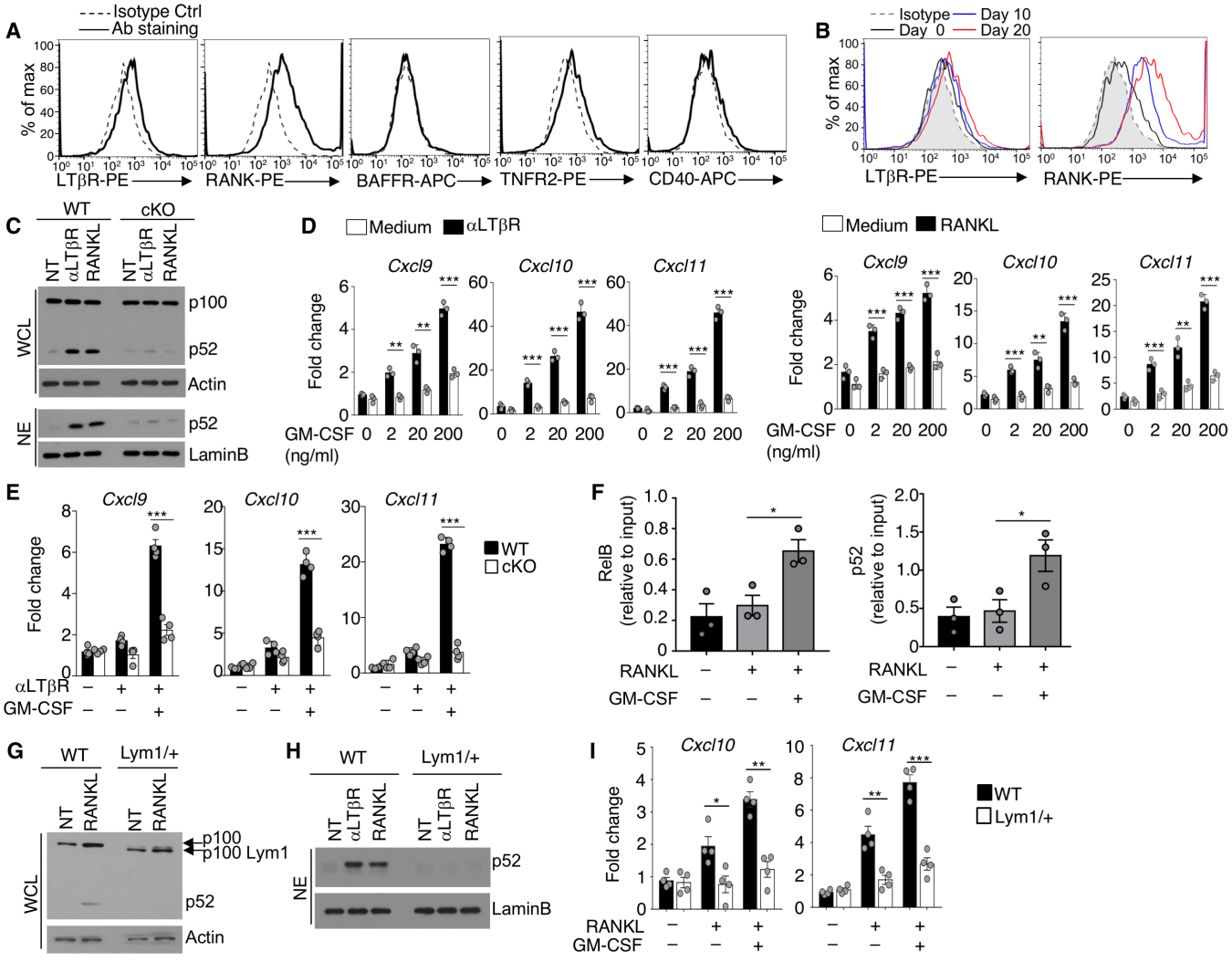

Fig. 5. Noncanonical NF-κB pathway mediates microglial chemokine expression in synergy with GM-CSF. (**A** and **B**) Flow cytometric analysis of the indicated TNFR superfamily members in microglia prepared from day 20 (A) or the indicated time points (B) of EAE induction. Ab, antibody. (**C**) Immunoblot analysis of p100 and its processing product p52 in whole-cell lysates and nuclear extracts of wild-type and *Map3k14*-cKO microglia that were either not treated (NT) or stimulated for 24 hours with the indicated agonists. (**D**) qRT-PCR analysis of the indicated mRNAs in wild-type microglia that were treated overnight with medium control, αLTβR, or RANKL and then stimulated for 2 hours with the indicated doses of GM-CSF. (**E**) qRT-PCR analysis of the indicated mRNAs in wild-type and *Map3k14*-cKO microglia that were either not treated (–) or stimulated (+) overnight with αLTβR, followed by a 2-hour stimulation with (+) or without (–) GM-CSF. (**F**) ChIP assays detecting the binding of RelB and p52 to the promoter region of the *Cxcl10* gene using microglia cultured overnight with (+) or without (–) RANKL, followed by a 2-hour stimulation with (+) or without (–) GM-CSF. (**G** and **H**) Immunoblot analysis of p100 and its processing product p52 in whole-cell lysates or nuclear extracts of wild-type and *Nfkb2*$^{lym1/+}$ microglia that were either not treated or stimulated for 24 hours with the indicated agonists. (**I**) qRT-PCR analysis of the indicated mRNAs in wild-type and *Nfkb2*$^{lym1/+}$ microglia that were either not treated (–) or stimulated (+) overnight with RANKL, followed by further stimulation for 2 hours with (+) or without (–) GM-CSF. Summary data are presented as means ± SEM, and *P* values were analyzed by two-tailed Student's *t* test (D to F and I). **P* < 0.05, ***P* < 0.01, and ****P* < 0.001.

regulation of inflammatory T cell infiltration into the CNS and EAE disease progression.

Precisely how Traf3 negatively regulates inflammation is unclear, although it has been implicated in the regulation of Toll-like receptor signaling (*32*). Since Traf3 serves as a negative regulator of NIK (*15*, *33*), we examined whether Traf3 might regulate microglial cell activation through controlling noncanonical NF-κB activation. The microglial cell–specific deletion of Traf3 profoundly enhanced p100 processing during EAE induction and increased the expression level of microglial activation markers, MHCII, CD80, CD40, and CD45 (Fig. 6, F and G). Furthermore, the Traf3 deficiency significantly promoted the expression of chemokines, including *cxcl9*, *cxcl10*, and *cxcl11*, in the microglia isolated from EAE mice (Fig. 6H). Traf3 deletion also rendered microglia responsive to chemokine gene induction in vitro by the cytokine GM-CSF (Fig. 6I). To further confirm the involvement of microglial NIK signaling axis in *Traf3*-mediated regulation of EAE, we generated mice harboring microglial cell–conditional deletion of both Traf3 and Map3k14 (Traf3/*Map3k14*-cKO) by treating the *Traf3*$^{fl/fl}$*Map3k14*$^{fl/fl}$ *Cx3Cr1*^{CreErt2} mice with tamoxifen as depicted in fig. S1A. While Traf3 deletion in microglia exacerbated EAE progression, simultaneous deletion of Traf3 and NIK completely reversed this phenotype

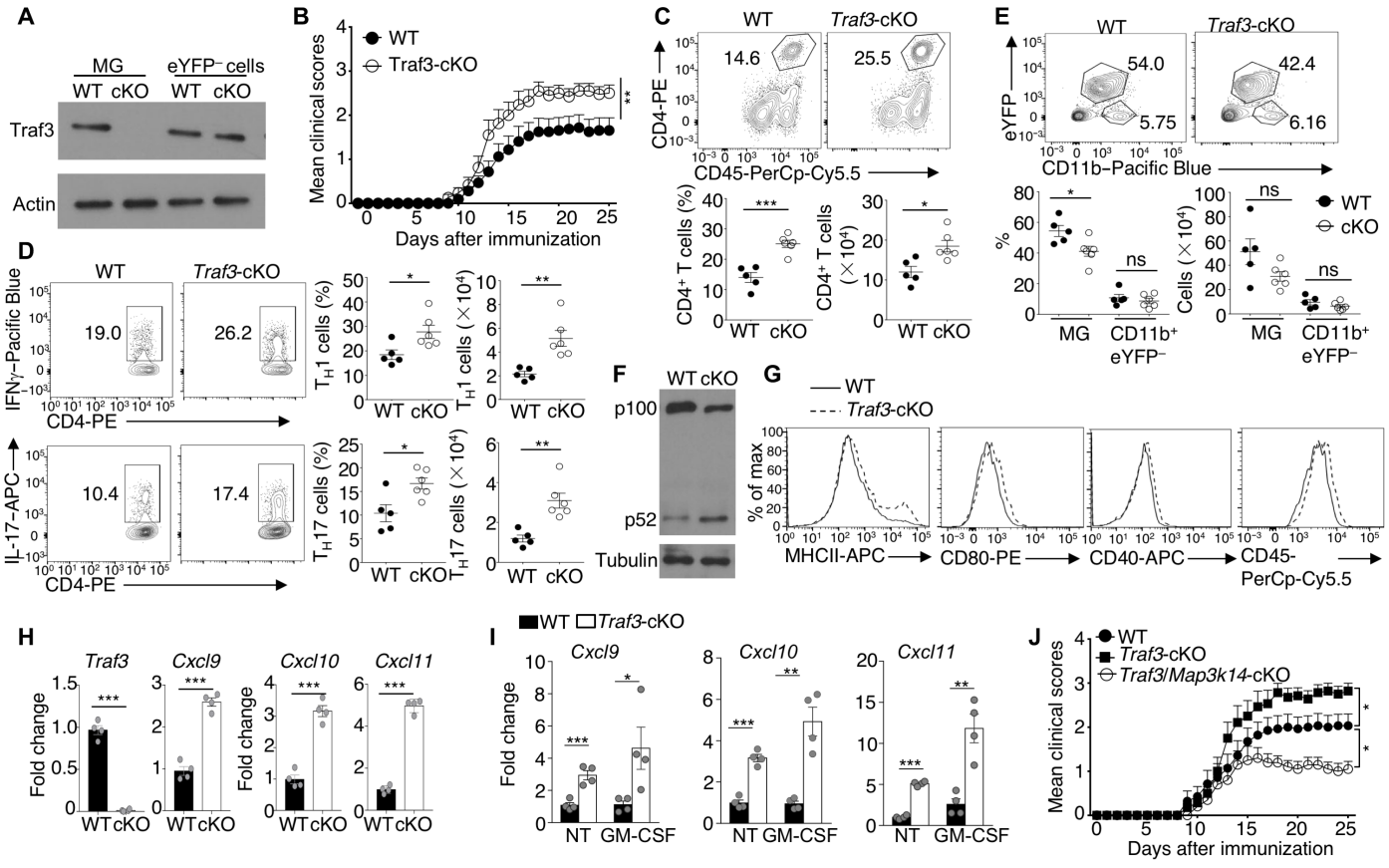

Fig. 6. Traf3 deficiency in microglia exacerbates EAE. (**A**) Immunoblot analysis of Traf3 and loading control actin in whole-cell extracts of microglia (eYFP$^+$CD11b$^+$) or eYFP$^-$CD11b$^+$ monocytes from the CNS of WT and *Traf3*-cKO (cKO) mice. (**B**) Mean clinical scores of age- and sex-matched wild-type and *Traf3*-cKO mice subjected to EAE induction by MOG_{35-55} immunization ($n = 16$ per group). (**C** to **E**) Flow cytometric analysis of CD4$^+$ T cells (C), T_H1 and T_H17 effector T cells (D), eYFP$^+$CD11b$^+$ microglia, and eYFP$^-$CD11b$^+$ monocytes (E) in the CNS (brain and spinal cord) of MOG_{35-55}-immunized WT and *Traf3*-cKO mice (WT, $n = 5$; *Traf3*-cKO, $n = 6$; day 25 after immunization). Data are presented as representative plots and summary graphs. (**F**) Immunoblot analysis of p100 and its processing product, p52, in whole-cell extracts of sorted microglia (CD11b$^+$eYFP$^+$ cells) from CNS of MOG_{35-55}-immunized wild-type and *Traf3*-cKO mice. (**G**) Flow cytometric analysis of surface activation markers in the microglia of EAE-induced wild-type and *Traf3*-cKO mice. (**H**) qRT-PCR analysis of the indicated mRNAs in freshly sorted microglia from MOG_{35-55}-immunized WT and *Traf3*-cKO mice ($n = 4$, day 25 after immunization). (**I**) qRT-PCR analysis of the indicated mRNAs in WT or *Traf3*-cKO microglia that were either not treated or stimulated for 2 hours with GM-CSF. (**J**) Mean clinical scores of age- and sex-matched wild-type, *Traf3*-cKO, and *Traf3*/*Map3k14*-cKO mice subjected to MOG_{35-55}-induced EAE (WT, $n = 14$; *Traf3*-cKO, $n = 14$; *Traf3*/*Map3k14*-cKO, $n = 10$). Data are representative of two (A, F, and H to J) or three (B to E and G) independent experiments. Summary data are presented as means ± SEM, and *P* values were determined by two-way ANOVA analysis (B and J) or two-tailed Student's *t* test (C to E, H, and I).*$P < 0.05$, **$P < 0.01$, and ***$P < 0.001$.

(Fig. 6J). These data suggest that microglial Traf3 negatively regulates EAE disease progression through controlling the NIK signaling axis.

Ectopic expression of NIK promotes microglial activation and EAE pathogenesis

Signal-induced NIK activation is mediated through its stabilization and accumulation (*15*). To further examine the role of NIK in regulating microglial function and EAE pathogenesis, we used a transgenic mouse model, R26Stop^{FL}*Map3k14*, carrying a *Map3k14* transgene under the control of a loxP-flanked STOP cassette (*34*). By crossing R26Stop^{FL}*Map3k14* mice with *Cx3Cr1*^{CreErt2} transgenic mice and subsequently treating the progeny mice with tamoxifen as depicted in fig. S1A, we generated microglial cell–conditional *Map3k14* transgenic (*Map3k14*-cTg) and wild-type control mice. As expected, transgenic expression of NIK promoted p100 processing in microglia along with EAE induction (Fig. 7A). Furthermore, ectopic expression of NIK in the *Map3k14*-cTg mice profoundly exacerbated EAE disease severity during the late phase, but not early phase (Fig. 7B). Consistently, the *Map3k14*-cTg mice had increased CNS infiltration with CD4$^+$ T cells, as well as T_H1 and T_H17 effector T cells (Fig. 7, C and D). Although ectopic NIK expression did not increase the microglial cell number, it promoted microglial activation as indicated by increased expression of the activated microglial marker Iba1 and morphology changes (Fig. 7, E and F). The microglia from the EAE-induced *Map3k14*-cTg mice also displayed increased expression levels of several other activation markers (Fig. 7G) and the chemokines *Cxcl9*, *Cxcl10*, and *Cxcl11* (Fig. 7H), compared to the microglia from EAE-induced wild-type mice. Thus, contrary to NIK deficiency, inducible expression of NIK in microglia promotes microglial activation and chemokine production, coupled with exacerbated EAE disease progression.

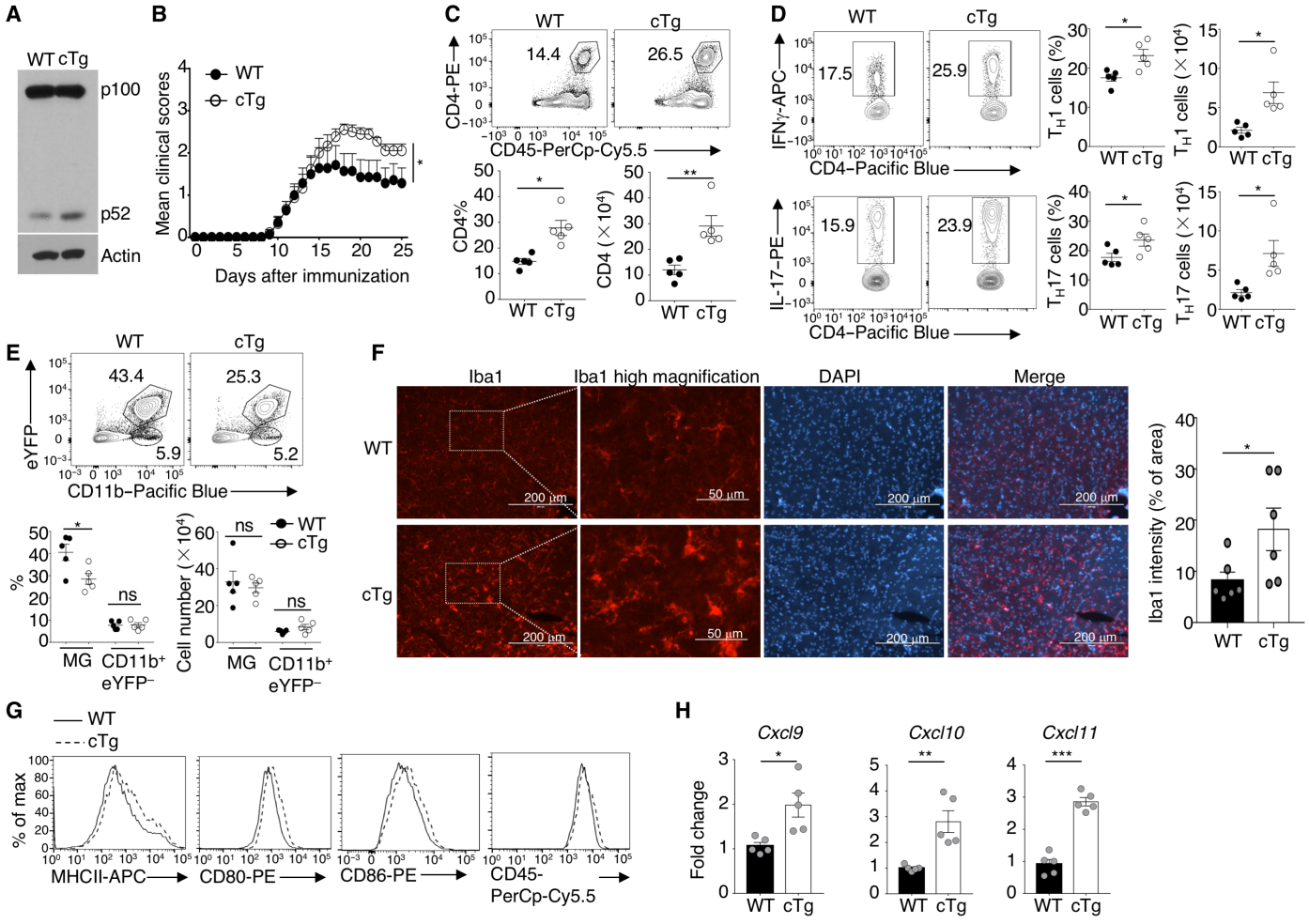

Fig. 7. Ectopic expression of NIK in microglia exacerbates late-phase EAE. (**A**) Immunoblot analysis of p100 and its processing product, p52, in whole-cell extracts of sorted microglia ($CD11b^+eYFP^+$ cells) from the CNS of $MOG_{35–55}$-immunized (day 25) WT and *Map3k14*-cTg (cTg) mice. (**B**) Mean clinical scores of age- and sex-matched wild-type and *Map3k14*-cTg mice subjected to $MOG_{35–55}$-induced EAE (WT, $n = 7$; *Map3k14*-cTg, $n = 9$). (**C** to **E**) Flow cytometric analysis of $CD4^+$ T cells (C), T_H1 and T_H17 effector T cells (D), $eYFP^+CD11b^+$ microglia, and $eYFP^-CD11b^+$ monocytes (E) in the CNS (brain and spinal cord) of $MOG_{35–55}$-immunized WT and *Map3k14*-cTg mice ($n = 5$, day 25 after immunization). Data are presented as representative plots and summary graphs. (**F**) Immunofluorescence staining of Iba1 and nuclei [with 4′,6-diamidino-2-phenylindole (DAPI)] of spinal cord sections of EAE-immunized (day 25) *Map3k14*-cKO or WT control mice. Data are shown as representative images (left) or a summary graph of Iba1 intensity (right). The Iba1 high-magnification panel shows the area in the square (**G**). Flow cytometric analysis of surface activation markers in the microglia of EAE-induced WT and *Map3k14*-cTg mice. (**H**) qRT-PCR analysis of the indicated mRNAs in freshly sorted microglia from $MOG_{35–55}$-immunized wild-type and *Map3k14*-cTg mice. Summary data are presented as means ± SEM, and *P* values are determined by two-way ANOVA analysis (B) or two-tailed Student's *t* test (C to F and H). $^*P < 0.05$, $^{**}P < 0.01$, and $^{***}P < 0.001$.

DISCUSSION

Data presented in this paper demonstrated a critical role for the NIK-directed noncanonical NF-κB pathway in regulating microglial function in EAE pathogenesis. Microglial NIK is dispensable for the initial phase of T cell infiltration into the CNS and EAE disease onset, but it is required for the subsequent CNS recruitment of T cells and disease progression. The microglial NIK signaling axis responds to stimulation by infiltrating T cells and mediates induction of microglial chemokines in synergy with the T cell cytokine GM-CSF, thereby promoting CNS recruitment of inflammatory T cells and monocytes during the late phase of EAE. These findings demonstrate a role for the NIK signaling axis in mediating microglial function and provide novel insight into the mechanism by which microglia regulate neuroinflammation.

Although microglia have been implicated in the pathogenesis of EAE and MS, how these CNS-resident macrophages are regulated and participate in the pathological process of CNS inflammation has been poorly understood. Our data suggest that microglial cell activation during EAE involves induction of the noncanonical NF-κB pathway. This pathway is not required for microglial expansion but supports the pathological function of microglia in sustaining CNS inflammation during EAE disease progression. Conditional deletion of NIK in microglia ameliorated late-phase EAE without affecting the initial phase disease severity, a finding consistent with the delayed kinetics of noncanonical NF-κB activation in microglia during EAE induction. It has been proposed that microglia interact with infiltrating T cells and mediate effector T cell restimulation by presenting myelin-specific antigens (*35*). Our data suggest that the

microglial cell–T cell interaction may also serve as a mechanism that triggers the NIK signaling axis in microglia. We found that microglia express members of the TNFR superfamily, most abundantly LTβR and RANK, which mediate noncanonical NF-κB activation. Since the ligands of these receptors, LTα1β2, LIGHT, and RANKL, are expressed by activated T cells, it is reasonable to propose that noncanonical NF-κB activation may occur during the microglia–T cell interaction. In support of this idea, adoptively transferred T_H17 cells activated noncanonical NF-κB signaling in microglia, and cocultivation of microglia with activated T cells in vitro also led to noncanonical NF-κB activation. Consistently, we found that microglial NIK is important for EAE induction by adoptively transferred T_H17 cells. T_H17 cell–mediated passive EAE induction is also impaired in the *Nfkb2*$^{lym1/+}$ recipient mice defective in noncanonical NF-κB activation. Compared to the passive EAE defect in *Map3k14*-cKO recipient mice, the EAE defect in *Nfkb2*$^{lym1/+}$ recipient mice is more notable. This difference is likely due to the whole-body noncanonical NF-κB defect of the *Nfkb2*$^{lym1/+}$ mice possibly affecting the function of both microglia and other cell types involved in EAE pathogenesis. The NIK pathway has been shown to mediate GM-CSF induction in T cells (*36*, *37*), although the contribution of endogenous T cells to passive EAE induction may not be significant since the recipient mice are sublethally irradiated to eliminate endogenous T cells. Future studies will examine whether the noncanonical NF-κB pathway functions in other CNS cells, such as astrocytes and neurons, in EAE regulation.

A hallmark of the encephalitogenic T_H1 and T_H17 cells is the production of the proinflammatory cytokine GM-CSF, which is critical for EAE induction (*27*–*29*). Notably, the T cell–derived GM-CSF is crucial for sustaining neuroinflammation during the effector phase of EAE and is thought to act through activating the invading myeloid cells (*29*). Our present study suggests a novel mechanism by which GM-CSF promotes CNS inflammation. In synergy with the noncanonical NF-κB inducers, GM-CSF stimulates microglia to produce chemokines known to mediate recruitment of inflammatory T cells and monocytic cells. However, our current findings could not prove whether GM-CSF is essential for in vivo microglial activation during EAE and whether additional cytokines could synergize with the noncanonical NF-κB pathway to induce chemokine expression in microglia. Nevertheless, on the basis of our findings, we propose a model of T cell–microglial cell interplay in mediating neuroinflammation. During the early phase of EAE induction, inflammatory T cells infiltrate into the CNS, where they stimulate noncanonical NF-κB signaling in microglia and secrete proinflammatory cytokines, including GM-CSF. The noncanonical NF-κB pathway synergizes with the GM-CSF signal to induce the expression of microglial chemokines that contribute to the second wave of T cell recruitment and EAE disease progression. Prior studies suggest that NIK also mediates EAE pathogenesis through facilitating the generation and function of T_H1 and T_H17 cells (*37*–*40*). NIK appears to exert this function via both T cell–intrinsic and dendritic cell–dependent mechanisms. These findings, along with our present study, implicate NIK as a potential target for the treatment of MS and other CNS inflammatory disorders.

We and others have previously shown that TRAF3 negatively regulates EAE induction, although the underlying mechanism has remained elusive (*12*, *31*). Our present study suggests that TRAF3 has a microglial cell–intrinsic function in EAE regulation. Furthermore, controlling the NIK signaling axis appears to be an important mechanism of TRAF3 action in microglia. Mice carrying microglial cell–conditional TRAF3 deficiency displayed an exacerbated EAE phenotype, which was reversed upon NIK deletion. However, the EAE phenotype of Traf3 deletion and NIK overexpression in microglia are not identical. While NIK overexpression selectively exacerbated the late-phase EAE, Traf3 deletion increased the disease severity during both the early and late phases. These results suggest that in addition to controlling the NIK signaling axis, Traf3 regulates the early-phase activation of microglia. In this regard, Traf3 has been shown to negatively regulate Toll-like receptor–stimulated expression of proinflammatory cytokines in microglia (*32*, *41*). In conclusion, our present study suggests the involvement of the NIK signaling axis in microglial function to sustain the CNS inflammation during the late-phase EAE. Our findings not only reveal a novel mechanism mediating the pathogenesis of EAE but also have implications for therapeutic approaches.

METHODS

Mice

Map3k14 flox mice (*42*), provided by Genentech, were crossed with *Cx3cr1*$^{CreER\text{-}eYFP}$ mice (the Jackson laboratory) (*19*) to produce age-matched *Map3k14*$^{+/+}$*Cx3cr1*$^{CreER\text{-}eYFP}$ and *Map3k14*$^{fl/fl}$*Cx3cr1*$^{CreER\text{-}eYFP}$ mice, which were then injected intraperitoneally with tamoxifen (2 mg per mouse) in corn oil daily for five consecutive days to induce Cre function for generation of wild-type and *Map3k14*-cKO mice. R26Stop^{FL}*Map3k14* NIK transgenic mice, carrying a *Map3k14* transgene encoding wild-type NIK under the control of a loxP-flanked STOP cassette (the Jackson laboratory) (*34*), were crossed with *Cx3cr1*$^{CreER\text{-}eYFP}$ mice (the Jackson laboratory) to generate *Map3k14*$^{+/+}$*Cx3cr1*$^{CreER\text{-}eYFP}$ and R26Stop^{FL}*Map3k14-Cx3cr1*$^{CreER\text{-}eYFP}$ mice, which were injected with tamoxifen to produce wild-type and microglial cell–conditional *Map3k14* transgenic (*Map3k14*-cTg) mice. *Traf3* flox mice (*43*), provided by R. Brink (Garvan Institute of Medical Research), were crossed with *Cx3cr1*$^{CreER\text{-}eYFP}$ mice (the Jackson laboratory) to generate *Traf3*$^{+/+}$*Cx3cr1*$^{CreER\text{-}eYFP}$ and *Traf3*$^{fl/fl}$*Cx3cr1*$^{CreER\text{-}eYFP}$, which were injected with tamoxifen to produce wild-type and *Traf3*-cKO mice. Mice with double deletion of *Traf3* and *Map3k14* in microglia (*Traf3*/*Map3k14*-cKO) were generated by generating *Traf3*$^{fl/fl}$*Map3k14*$^{fl/fl}$*Cx3cr1*$^{CreER\text{-}eYFP}$ mice and subsequent injection with tamoxifen. *Nfkb2*^{lym1} mice were provided by R. Starr and the Walter and Eliza Hall Institute of Medical Research (*30*). *Nfkb2*$^{lym1/+}$ heterozygous mice were used in experiments since they display strong phenotype in impaired noncanonical NF-κB activation and function (*30*). Experiments were performed with age- and sex-matched mice. All mice were on C57BL/6 genetic background and maintained in a specific pathogen–free facility of the University of Texas MD Anderson Cancer Center, and all animal experiments were carried out in accordance with protocols approved by the Institutional Animal Care and Use Committee of the University of Texas MD Anderson Cancer Center.

Antibodies and reagents

The following fluorochrome-labeled antibodies specific to mouse (m) proteins and their corresponding isotype controls were purchased from eBioscience (San Diego, CA): APC- or phycoerythrin (PE)–conjugated anti–mIL-17A (eBio17B7), fluorescein isothiocyanate (FITC)– or APC-conjugated anti-mIFNγ (XMG1.2), FITC-conjugated anti–mGM-CSF (MP1-22E9), APC-conjugated anti-mFoxp3 (FJK-16 s), PE-Cy7–conjugated anti-mCD3 (17A2), PE- or Pacific Blue–conjugated

anti-mCD4 (GK1.5), Pacific Blue–conjugated anti-mCD11b (M1/70), PE- or PerCp-Cy5.5–conjugated anti-mCD45 (30-F11), FITC-conjugated anti-mCD45.1 (A20), APC- or PE-Cy7–conjugated anti-mCD45.2 (104), PE- or FITC-conjugated anti-mCD80 (16-10A1), PE- or FITC-conjugated anti-mCD86 (GL1), APC-conjugated anti-mMHCII (M5/114.15.2), APC- or PE-conjugated anti-mCD40 (HM40-3), APC-conjugated anti-mCXCR3 (CXCR3-173), PE-conjugated anti-mCCR5 (HM-CCR5), PE-conjugated anti-mRANK (R12-31), PE-conjugated mBAFF receptor (8A7), and PE-conjugated anti-mLTβR (ebio3C8). Purified anti-mCD16/32 (2.4G2), APC-conjugated anti-mCCR6 (140706), and PE-conjugated anti-mCD120b (TR75-89) were purchased from BD Pharmingen. PE-conjugated anti-mCX_3CR1 (SA011F11) was purchased from BioLegend.

Anti-actin (C-4; 1:10,000) was from Sigma-Aldrich. Antibodies for anti-p100/p52 (1:1000) and α-tubulin (1:1000) were from Cell Signaling Technology. Anti–lamin B (1:1000) was from Abcam. Anti-mouse LTβR was from Bio-Rad. Recombinant murine GM-CSF was from PeproTech, and recombinant murine RANKL was from the R&D System.

Induction and assessment of EAE

Active EAE was induced as previously described (*38*). EAE induction was performed with age- and sex-matched mice. Briefly, mice were injected subcutaneously with the $MOG_{35–55}$ peptide (200 μg) in Complete Freund's Adjuvant (CFA) containing heat-killed *Mycobacterium tuberculosis* (5 mg/ml; H37Ra strain, BD Diagnostics). On the day of immunization and 48 hours later, mice were injected intraperitoneally with Pertussis toxin (200 ng per mouse; List Biological Laboratories). Mice were examined daily for EAE disease symptoms, which were scored using a standard method: 0, no clinical signs; 1, limp tail; 2, paraparesis (weakness, incomplete paralysis of one or two hind limbs); 3, paraplegia (complete paralysis of two hind limbs); 4, paraplegia with fore limb weakness or paralysis; 5, moribund state or death. The EAE scores were accessed without group allocation information.

For passive EAE, B6.SJL mice ($CD45.1^+$) were immunized with $MOG_{35–55}$ peptide for 10 days. Draining lymph node and spleen cells were isolated and in vitro expanded for 72 hours in the presence of $MOG_{35–55}$ (50 μg/ml) in the presence of IL-23 and IL-1β (for generating T_H17 cells). The MOG-specific T_H17 cells were adoptively transferred into sublethally irradiated (5 gray; 12 hours after irradiation) wild-type and *Map3k14*-cKO mice. Mice were examined daily for EAE disease symptoms and scored using a standard method as described above.

In vitro cultivation and activation of primary microglia

The meninges of the brains from newborn mice (1 to 3 days of age) were carefully removed. Brain tissue was digested using trypsin and deoxyribonuclease I (DNase I) at 37°C and filtered with a 70-μm mesh, and the cells were cultured in Dulbecco's modified Eagle's medium (DMEM)–F12 medium supplemented with 10% fetal bovine serum, 1% penicillin/streptavidin and glutamine. Cell suspension was incubated in cell culture dish pretreated with poly-L-lysine. After 2 weeks of cultivation (with medium changes at 24 hours and then every 4 days), the adherent astrocytes were removed by mild trypsinization for 30 min (*44*). Microglia were collected and resuspended in DMEM–F12 medium for further analysis. The purity of the isolated microglia was around 99% as determined by flow cytometry analysis (fig. S4B). To induce Cre-mediated gene deletion in vitro, mixed glial cells prepared from newborn mice carrying $Cx3cr1^{CreER\text{-}eYFP}$ were stimulated with 1 μM 4-hydroxytamoxifen (Sigma-Aldrich) for 5 days before purification of microglia by mild trypsinization.

Microglia were seeded in six-well plates and stimulated for 24 hours with anti-LTβR (1 μg/ml) or RANKL (50 ng/ml) and subjected to immunoblot analysis of p100 processing. For chemokine induction, microglia were stimulated overnight with anti-LTβR or RANKL and then stimulated for 2 hours with different doses of GM-CSF (20 ng/ml). For T cell–mediated microglial activation, 3×10^6 of microglia were seeded for 24 hours in a six-well plate. At the same day, $CD4^+$ T cells were isolated and activated for 24 hours with plated-bound anti-CD3 and anti-CD28. The microglial cells were then co-cultured for additional 24 hours with the activated $CD4^+$ T cells at the indicated ratios. The cell culture plate was washed three times with phosphate-buffered saline (PBS) to remove the T cells in suspension, and the attached microglia were harvested and further purified by flow cytometric cell sorting (based on CD11b expression) using a BD FACSAria cell sorter.

Preparation of microglia from adult mice

Adult mouse microglia were isolated as described previously (*45*). Briefly, mice were euthanized and perfused with cold PBS. Brains and spinal cords were then rinsed, minced, and digested with collagenase IV (0.5 mg/ml; Sigma-Aldrich) and DNase I (100 μg/ml; Roche) in RPMI 1640. Dispersed cells were passed through a 70-μm mesh and collected by centrifugation. Cell suspension was layered onto a Percoll density gradient and centrifuge for 40 min (300*g*) at room temperature. CNS leukocytes were isolated by collection of the interface fraction between 37 and 70% interphase. Cells were thoroughly washed and resuspended in completed RPMI 1640 containing 10% fetal bovine serum. CNS leukocytes were further stained with APC-conjugated anti-mCD45 and Pacific Blue–conjugated anti-mCD11b. Microglia were sorted as $CD45^+CD11b^+eYFP^+$ cells using FACSJazz.

Isolation and analysis of CNS mononuclear cells

Mice were harvested for CNS infiltration analysis at the indicated times after $MOG_{35–55}$ immunization. After perfusion, the brains and spinal cords were excised, minced, and digested with collagenase IV (0.5 mg/ml; Sigma-Aldrich) and DNase I (100 μg/ml; Roche) for 40 min at 37°C. After digestion, cell suspensions were passed through 70-μm cell strainer to yield single-cell suspensions. CNS mononuclear cells were purified by centrifugation (400*g*) at room temperature for 30 min over a 30/70% discontinuous Percoll gradient. The cells were collected from the interphase, thoroughly washed, and analyzed by flow cytometry.

Histological analysis

We dissected spinal cords from mice transcardially perfused with 4% paraformaldehyde and postfixed them overnight. We then stained the paraffin-embedded sections (8 μm) of spinal cords with hemotoxylin and eosin (H&E) for visualizing leukocyte infiltration or with Luxol Fast Blue (LFB) for assessing demyelination.

Flow cytometry and intracellular cytokine staining

Flow cytometry and intracellular cytokine staining (ICS) were performed following procedures previously described (*46*). Briefly, single-cell suspensions were prepared from the indicated tissues and subjected to flow cytometry using an LSRFortessa (Becton Dickinson, San Jose, CA). The cells were incubated with anti-CD16/CD32 (eBioscience)

to block nonspecific antibody binding via Fc receptors, then stained with fluorochrome-labeled antibodies, and subsequently processed on an LSRFortessa. The data were analyzed using FlowJo software (Tree Star, Ashland, OR), and gating strategy is shown in fig. S8. For ICS detection of IFNγ, IL-17, and GM-CSF, cells were stimulated for 4 to 5 hours with phorbol 12-myristate 13-acetate (50 ng/ml) and ionomycin (750 ng/ml) in the presence of GolgiStop (BD Biosciences). After incubation, cells were stained with fixable viability dye, blocked with FcγR blocker (CD16/32), and stained for specific surface molecules. After surface staining, cells were fixed, permeabilized, and stained for intracellular cytokines by using a fixation/permeabilization kit (BD Biosciences). Samples were processed on an LSRII FACSFortessa (Becton Dickinson, San Jose, CA) and analyzed by using FlowJo software (TreeStar, Ashland, OR).

Real-time qRT-PCR

Real-time qRT-PCR was performed as previously described (*46*). Total RNA was isolated from microglia cells using TRI reagent (Invitrogen) and subjected to complementary DNA synthesis using Moloney Murine Leukemia Virus (MMLV) reverse transcriptase (Invitrogen) and oligo(dT) primers. Real-time qRT-PCR was performed using the iCycler Sequence Detection System (Bio-Rad, Hercules, CA) and iQ SYBR Green Supermix (Bio-Rad). The expression of individual genes was calculated by a standard curve method and was normalized to the expression of β-actin. The primers used in qRT-PCR assays are shown in table S1.

Immunoblotting

Whole-cell and subcellular extracts were prepared and subjected to immunoblotting essentially as described (*46*). Briefly, protein samples were separated by SDS–polyacrylamide gel electrophoresis, transferred to polyvinylidene difluoride membranes (0.45 μm; Millipore), and blocked for 1 hour with 5% bovine serum albumin (BSA) and 0.1% Tween 20 in tris-buffered saline. The membranes were then washed and incubated with primary antibodies overnight. The goat anti-rabbit or goat anti-mouse immunoglobulin G secondary antibodies (1:5000 dilution) were used to incubate for 1 hour. After washing, immunoreactive bands were visualized by chemiluminescent detection (ECL, Roche Diagnostics, Penzberg, Germany) and exposure to x-ray film (Thermo Fisher Scientific, MA, US).

ChIP assay

Naïve microglia cells were either not treated or stimulated overnight with RANKL, followed by a 2-hour stimulation with or without GM-CSF. ChIP assay was performed using the EpiQuik ChIP Kit (EpiGentek, catalog no. P-2002-03) and antibodies for Relb (Cell Signaling Technology, catalog no. 10544S) and p100/p52 (Cell Signaling Technology, catalog no. 4882S). The precipitated and purified DNA was then quantified by qPCR using specific primers that amplify the CXCL10 promoter (forward, GGGAGAGGGAAATTCCA; reverse, TTTCCCTCCCTGAGTCC). The *y* axis is the ratio of target transcript factor–binding DNA normalization to total input DNA.

Immunofluorescence staining

Spinal cords of the indicated mice were fixed in 4% paraformaldehyde at 4°C overnight and then cryoprotected in a 30% sucrose solution for 24 hours at 4°C. Tissues were embedded in optimal cutting temperature compound for frozen section. The sections were permeabilized for 10 min using 0.5% Triton X-100 in PBS and then blocked with 1% normal goat serum and 1% BSA in PBS for 2 hours at room temperature. Samples were stained with anti-Iba1 primary antibody for 48 hours at 4°C (1:250; Wako). After washed five times with 0.1% Triton X-100 in PBS, the sections were incubated for 1 hour with secondary Alexa Fluor 594–conjugated rabbit antibodies. Nuclei were counterstained with 4njugated rabbit antibodies. (DAPI). Slides were examined and photographed using an Olympus DP70 fluorescence microscope. The positive area of Iba1 was measured using ImageJ software and analyzed using GraphPad Prism 7.

Statistical analysis

Statistical analysis was performed using GraphPad Prism software (GraphPad). Significant differences between two groups were analyzed with two-tailed unpaired *t* test. For the EAE clinical scores, differences between groups were evaluated by two-way analysis of variance (ANOVA). *P* values less than 0.05 were considered significant, and the level of significance was indicated as $*P < 0.05$, $**P < 0.01$, and $***P < 0.001$. In the animal studies, four mice are required for each group based on the calculation to achieve a 2.3-fold change (effect size) in two-tailed Student's *t* test with 90% power and a significance level of 5%. All statistical tests are justified as appropriate, and data meet the assumptions of the tests. The variance is similar between the groups being statistically compared.

SUPPLEMENTARY MATERIALS

Supplementary material for this article is available at https://science.org/doi/10.1126/sciadv.abh0609

View/request a protocol for this paper from *Bio-protocol*.

REFERENCES AND NOTES

1. M. Filippi, A. Bar-Or, F. Piehl, P. Preziosa, A. Solari, S. Vukusic, M. A. Rocca, Multiple sclerosis. *Nat. Rev. Dis. Primers.* **4**, 43 (2018).
2. S. Glatigny, E. Bettelli, Experimental autoimmune encephalomyelitis (EAE) as animal models of multiple sclerosis (MS). *Cold Spring Harb. Perspect. Med.* **8**, a028977 (2018).
3. E. Pierson, S. B. Simmons, L. Castelli, J. M. Goverman, Mechanisms regulating regional localization of inflammation during CNS autoimmunity. *Immunol. Rev.* **248**, 205–215 (2012).
4. A. C. Murphy, S. J. Lalor, M. A. Lynch, K. H. Mills, Infiltration of Th1 and Th17 cells and activation of microglia in the CNS during the course of experimental autoimmune encephalomyelitis. *Brain Behav. Immun.* **24**, 641–651 (2010).
5. J. Zepp, L. Wu, X. Li, IL-17 receptor signaling and T helper 17-mediated autoimmune demyelinating disease. *Trends Immunol.* **32**, 232–239 (2011).
6. J. Correale, The role of microglial activation in disease progression. *Mult. Scler.* **20**, 1288–1295 (2014).
7. Z. Gao, S. E. Tsirka, Animal models of MS reveal multiple roles of microglia in disease pathogenesis. *Neurol. Res. Int.* **2011**, 383087 (2011).
8. S. T. T. Schetters, D. Gomez-Nicola, J. J. Garcia-Vallejo, Y. Van Kooyk, Neuroinflammation: Microglia and T cells get ready to tango. *Front. Immunol.* **8**, 1905 (2017).
9. F. Ginhoux, M. Greter, M. Leboeuf, S. Nandi, P. See, S. Gokhan, M. F. Mehler, S. J. Conway, L. G. Ng, E. R. Stanley, I. M. Samokhvalov, M. Merad, Fate mapping analysis reveals that adult microglia derive from primitive macrophages. *Science* **330**, 841–845 (2010).
10. K. Saijo, C. K. Glass, Microglial cell origin and phenotypes in health and disease. *Nat. Rev. Immunol.* **11**, 775–787 (2011).
11. A. Crotti, R. M. Ransohoff, Microglial physiology and pathophysiology: Insights from genome-wide transcriptional profiling. *Immunity* **44**, 505–515 (2016).
12. Y. Xiao, J. Jin, M. Chang, J. H. Chang, H. Hu, X. Zhou, G. C. Brittain, C. Stansberg, O. Torkildsen, X. Wang, R. Brink, X. Cheng, S. C. Sun, Peli1 promotes microglia-mediated CNS inflammation by regulating Traf3 degradation. *Nat. Med.* **19**, 595–602 (2013).
13. L. Ting, L. Zhang, D. Joo, S. C. Sun, NF-κB signaling in inflammation. *Signal Transduct. Target Ther.* **2**, 17023 (2017).
14. S. C. Sun, The non-canonical NF-κB pathway in immunity and inflammation. *Nat. Rev. Immunol.* **17**, 545–558 (2017).
15. S. C. Sun, The noncanonical NF-κB pathway. *Immunol. Rev.* **246**, 125–140 (2012).
16. G. Xiao, E. W. Harhaj, S. C. Sun, NF-κB-inducing kinase regulates the processing of NF-κB2 p100. *Mol. Cell* **7**, 401–409 (2001).
17. U. Senftleben, Y. Cao, G. Xiao, G. Krähn, F. R. Greten, G. Bonizzi, Y. Chen, Y. Hu, A. Fong, S.-C. Sun, M. Karin, Activation by IKKα of a second, evolutionary conserved, NF-κB signaling pathway. *Science* **293**, 1495–1499 (2001).

18. E. Dejardin, The alternative NF-κB pathway from biochemistry to biology: Pitfalls and promises for future drug development. *Biochem. Pharmacol.* **72**, 1161–1179 (2006).
19. C. N. Parkhurst, G. Yang, I. Ninan, J. N. Savas, J. R. Yates III, J. J. Lafaille, B. L. Hempstead, D. R. Littman, W.-B. Gan, Microglia promote learning-dependent synapse formation through brain-derived neurotrophic factor. *Cell* **155**, 1596–1609 (2013).
20. A. Reboldi, C. Coisne, D. Baumjohann, F. Benvenuto, D. Bottinelli, S. Lira, A. Uccelli, A. Lanzavecchia, B. Engelhardt, F. Sallusto, C-C chemokine receptor 6-regulated entry of T_H-17 cells into the CNS through the choroid plexus is required for the initiation of EAE. *Nat. Immunol.* **10**, 514–523 (2009).
21. R. Sporici, T. B. Issekutz, CXCR3 blockade inhibits T-cell migration into the CNS during EAE and prevents development of adoptively transferred, but not actively induced, disease. *Eur. J. Immunol.* **40**, 2751–2761 (2010).
22. O. M. Koper, J. Kamińska, K. Sawicki, H. Kemona, CXCL9, CXCL10, CXCL11, and their receptor (CXCR3) in neuroinflammation and neurodegeneration. *Adv. Clin. Exp. Med.* **27**, 849–856 (2018).
23. S. M. Gu, M. H. Park, H. M. Yun, S. B. Han, K. W. Oh, D. J. Son, J. S. Yun, J. T. Hong, CCR5 knockout suppresses experimental autoimmune encephalomyelitis in C57BL/6 mice. *Oncotarget* **7**, 15382–15393 (2016).
24. W. J. Karpus, Cytokines and chemokines in the pathogenesis of experimental autoimmune encephalomyelitis. *J. Immunol.* **204**, 316–326 (2020).
25. R. Wang, L. Zhang, X. Zhang, J. Moreno, C. Celluzzi, M. Tondravi, Y. Shi, Regulation of activation-induced receptor activator of NF-κB ligand (RANKL) expression in T cells. *Eur. J. Immunol.* **32**, 1090–1098 (2002).
26. P. Stopfer, D. N. Mannel, T. Hehlgans, Lymphotoxin-β receptor activation by activated T cells induces cytokine release from mouse bone marrow-derived mast cells. *J. Immunol.* **172**, 7459–7465 (2004).
27. J. L. McQualter, R. Darwiche, C. Ewing, M. Onuki, T. W. Kay, J. A. Hamilton, H. H. Reid, C. C. Bernard, Granulocyte macrophage colony-stimulating factor: A new putative therapeutic target in multiple sclerosis. *J. Exp. Med.* **194**, 873–882 (2001).
28. E. D. Ponomarev, L. P. Shriver, K. Maresz, J. Pedras-Vasconcelos, D. Verthelyi, B. N. Dittel, GM-CSF production by autoreactive T cells is required for the activation of microglial cells and the onset of experimental autoimmune encephalomyelitis. *J. Immunol.* **178**, 39–48 (2007).
29. L. Codarri, G. Gyulveszi, V. Tosevski, L. Hesske, A. Fontana, L. Magnenat, T. Suter, B. Becher, RORγt drives production of the cytokine GM-CSF in helper T cells, which is essential for the effector phase of autoimmune neuroinflammation. *Nat. Immunol.* **12**, 560–567 (2011).
30. E. Tucker, K. O'Donnell, M. Fuchsberger, A. A. Hilton, D. Metcalf, K. Greig, N. A. Sims, J. M. Quinn, W. S. Alexander, D. J. Hilton, B. T. Kile, D. M. Tarlinton, R. Starr, A novel mutation in the *Nfkb2* gene generates an NF-κB2 "super repressor". *J. Immunol.* **179**, 7514–7522 (2007).
31. S. Zhu, W. Pan, P. Shi, H. Gao, F. Zhao, X. Song, Y. Liu, L. Zhao, X. Li, Y. Shi, Y. Qian, Modulation of experimental autoimmune encephalomyelitis through TRAF3-mediated suppression of interleukin 17 receptor signaling. *J. Exp. Med.* **207**, 2647–2662 (2010).
32. P.-H. Tseng, A. Matsuzawa, W. Zhang, T. Mino, D. A. Vignali, M. Karin, Different modes of ubiquitination of the adaptor TRAF3 selectively activate the expression of type I interferons and proinflammatory cytokines. *Nat. Immunol.* **11**, 70–75 (2010).
33. G. Liao, M. Zhang, E. W. Harhaj, S. C. Sun, Regulation of the NF-κB-inducing kinase by tumor necrosis factor receptor-associated factor 3-induced degradation. *J. Biol. Chem.* **279**, 26243–26250 (2004).
34. Y. Sasaki, D. P. Calado, E. Derudder, B. Zhang, Y. Shimizu, F. Mackay, S. Nishikawa, K. Rajewsky, M. Schmidt-Supprian, NIK overexpression amplifies, whereas ablation of its TRAF3-binding domain replaces BAFF:BAFF-R-mediated survival signals in B cells. *Proc. Natl. Acad. Sci. U.S.A.* **105**, 10883–10888 (2008).
35. Y. Dong, V. W. Yong, When encephalitogenic T cells collaborate with microglia in multiple sclerosis. *Nat. Rev. Neurol.* **15**, 704–717 (2019).
36. C. Sanchez-Valdepenas, A. G. Martin, P. Ramakrishnan, D. Wallach, M. Fresno, NF-κB-Inducing kinase is involved in the activation of the CD28 responsive element through phosphorylation of c-Rel and regulation of its transactivating activity. *J. Immunol.* **176**, 4666–4674 (2006).
37. J. Yu, X. Zhou, M. Nakaya, W. Jin, X. Cheng, S.-C. Sun, T cell-intrinsic function of the noncanonical NF-κB pathway in the regulation of GM-CSF expression and experimental autoimmune encephalomyelitis pathogenesis. *J. Immunol.* **193**, 422–430 (2014).
38. W. Jin, X. F. Zhou, J. Yu, X. Cheng, S. C. Sun, Regulation of Th17 cell differentiation and EAE induction by MAP3K NIK. *Blood* **113**, 6603–6610 (2009).
39. J. Hofmann, F. Mair, M. Greter, M. Schmidt-Supprian, B. Becher, NIK signaling in dendritic cells but not in T cells is required for the development of effector T cells and cell-mediated immune responses. *J. Exp. Med.* **208**, 1917–1929 (2011).
40. Y. Li, H. Wang, X. Zhou, X. Xie, X. Chen, Z. Jie, Q. Zou, H. Hu, L. Zhu, X. Cheng, H. D. Brightbill, L. C. Wu, L. Wang, S. C. Sun, Cell intrinsic role of NF-κB-inducing kinase in regulating T cell-mediated immune and autoimmune responses. *Sci. Rep.* **6**, 22115 (2016).
41. H. Hacker, P. H. Tseng, M. Karin, Expanding TRAF function: TRAF3 as a tri-faced immune regulator. *Nat. Rev. Immunol.* **11**, 457–468 (2011).
42. H. D. Brightbill, J. K. Jackman, E. Suto, H. Kennedy, C. Jones III, S. Chalasani, Z. Lin, L. Tam, M. Roose-Girma, M. Balazs, C. D. Austin, W. P. Lee, L. C. Wu, Conditional deletion of NF-κB–inducing kinase (NIK) in adult mice disrupts mature B cell survival and activation. *J. Immunol.* **195**, 953–964 (2015).
43. S. Gardam, F. Sierro, A. Basten, F. Mackay, R. Brink, TRAF2 and TRAF3 signal adapters act cooperatively to control the maturation and survival signals delivered to B cells by the BAFF receptor. *Immunity* **28**, 391–401 (2008).
44. J. Saura, J. M. Tusell, J. Serratosa, High-yield isolation of murine microglia by mild trypsinization. *Glia* **44**, 183–189 (2003).
45. A. E. Cardona, D. Huang, M. E. Sasse, R. M. Ransohoff, Isolation of murine microglial cells for RNA analysis or flow cytometry. *Nat. Protoc.* **1**, 1947–1951 (2006).
46. Z. Jie, J. Y. Yang, M. Gu, H. Wang, X. Xie, Y. Li, T. Liu, L. Zhu, J. Shi, L. Zhang, X. Zhou, D. Joo, H. D. Brightbill, Y. Cong, D. Lin, X. Cheng, S. C. Sun, NIK signaling axis regulates dendritic cell function in intestinal immunity and homeostasis. *Nat. Immunol.* **19**, 1224–1235 (2018).

Acknowledgments: We thank Genentech Inc. for providing *Map3k14* flox mice, Walter and Eliza Hall Institute of Medical Research for *Nfkb2*^{Lym1} mice, and R Brink for *Traf3* flox mice. We also thank the flow cytometry and animal facility of the shared resources at the MD Anderson Cancer Center, supported by the NIH/NCI Cancer Center Support Grant (CCSG) P30CA016672. **Funding:** This study was supported by NIH grant GM84459 to S.-C.S. and partially supported by NIH grant NS079166 to S.-J.T. T.G. was a visiting student supported by a scholarship from the China Scholarship Council with the grant number of 201906380080. **Author contributions:** Z.J. designed and performed the research, prepared the figures, and wrote the manuscript. C.-J.K. designed and performed the research and prepared the figures. H.W. initiated this project and performed the experiments. X.X., Y.L., M.G., L.Z., J.-Y.Y., and T.G. assisted with animal experiments, sample processing, and/or data analysis. W.R. and S.-J.T. provided expertise and technical advice on microglial experiments. X.C. assisted with animal experiments. S.-C.S. supervised the work and wrote the manuscript. **Competing interests:** The authors declare that they have no competing interests. **Data and materials availability:** All data needed to evaluate the conclusions in the paper are present in the paper and/or the Supplementary Materials. Materials can be provided by the authors pending a completed material transfer agreement. Requests for materials should be submitted to S.-C.S.

Submitted 12 February 2021
Accepted 14 July 2021
Published 3 September 2021
10.1126/sciadv.abh0609

Citation: Z. Jie, C.-J. Ko, H. Wang, X. Xie, Y. Li, M. Gu, L. Zhu, J.-Y. Yang, T. Gao, W. Ru, S.-J. Tang, X. Cheng, S.-C. Sun, Microglia promote autoimmune inflammation via the noncanonical NF-κB pathway. *Sci. Adv.* **7**, eabh0609 (2021).